NANO LETTERS

Letter

pubs.acs.org/NanoLett

Toroidal Plasmonic Eigenmodes in Oligomer Nanocavities for the Visible

Burcu Ögüt,*[,†] Nahid Talebi,[†] Ralf Vogelgesang,[‡] Wilfried Sigle,[†] and Peter A. van Aken[†]

[†]Max Planck Institute for Intelligent Systems, Heisenbergstraße 3, 70569 Stuttgart, Germany

[‡]Max Planck Institute for Solid State Research, Heisenbergstraße 1, 70569 Stuttgart, Germany

Supporting Information

ABSTRACT: Plasmonics has become one of the most vibrant areas in research with technological innovations impacting fields from telecommunications to medicine. Many fascinating applications of plasmonic nanostructures employ electric dipole and higher-order multipole resonances. Also magnetic multipole resonances are recognized for their unique properties. Besides these multipolar modes that easily radiate into free space, other types of electromagnetic resonances exist, so-called toroidal eigenmodes, which have been largely overlooked historically. They are strongly bound to material structures and their peculiar spatial structure renders them practically invisible to conventional optical microscopy techniques. In this Letter, we demonstrate toroidal modes in a metal ring formed by an oligomer of holes. Combined energy-filtering transmission electron microscopy and three-dimensional finite difference time domain analysis reveal their distinct features. For the study of these modes that cannot be excited by optical far-field spectroscopy, energy-filtering transmission electron microscopy emerges as the method of choice. Toroidal moments bear great potential for novel applications, for example, in the engineering of Purcell factors of quantum-optical emitters inside toroidal cavities.

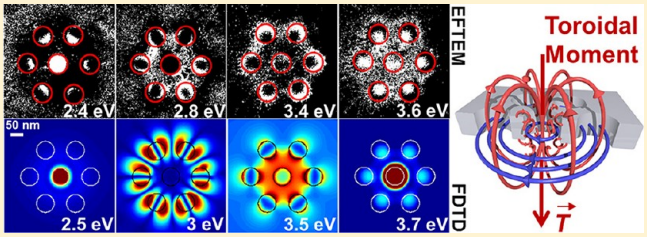

KEYWORDS: *Energy-filtering TEM, 3D finite-difference time-domain, toroidal eigenmodes, oligomers, plasmonics, nanocavities*

The inevitable trend of miniaturization in electronic devices has introduced an epoch for the young field of plasmonics, holding the attention of biological[1,2] and chemical[3] research, surface enhanced Raman Spectroscopy,[4] solar energy,[5] telecommunication technology,[6] and transformation optics.[7] It has become a vital issue to visualize and understand how the avant-garde class of materials designed for these applications behave electromagnetically in terms of electromagnetic field concentration and coupling in the optical wavelength regime. Therefore different imaging techniques[8] have been applied to nanoparticles and nanoholes[9] with different geometrical shapes, such as triangles,[10] spheres,[11,12] rods,[13] or split-rings.[14] Predominantly, electrical and magnetic dipolar and higher order resonances have been taken into consideration while studying these structures. However, toroidal moments represent a category of magnetoelectric moments by themselves, which are mostly disregarded as they are not so straightforward to detect, especially in nanoscale structures.

Starting from the late 1950s,[15] toroidal moments $\vec{T}$ have been studied at first in nuclear physics.[16] They are characterized by rings of radial electric field loops, $\vec{E}$, as depicted in Figure 1g, which is in contrast to the azimuthal field loop that generates the magnetic field component $\vec{H}$ of a simple ring. Toroidal polarizations are rare but possible in the solid state, as well. Recently, multiferroic materials have been discovered that even support ferrotoroidic domains.[17] A key feature in all occurrences of toroidal moments is space−time symmetry. Electric dipoles ($\vec{P} = \sum_i q_i \vec{r}_i$) change their sign only with space inversion ($\vec{r} \rightarrow -\vec{r}$) and magnetic dipoles ($\vec{m} = \sum_i q_i \vec{r}_i \times d\vec{r}_i/dt$) change their sign only with time reversal ($t \rightarrow -t$). Toroidal moments

$$\vec{T} = \sum_i q_i \vec{r}_i \times \left(\vec{r}_i \times \frac{d\vec{r}_i}{dt} \right) \quad (1)$$

however, swap their sign under either spatial inversion or time reversal.[18] A well-known example of a structure exhibiting a toroidal moment is a solenoid that is bent into a ring, or equivalently, a closed loop of azimuthally oriented magnetic moments. This behavior hints at an intricate coupling between ordinary electric and magnetic dipoles, as is indeed the case in the magnetoelectric effect. The hybrid nature of toroidal moments introduces options to influence magnetic polarization by electric fields and vice versa.[19]

Even though toroidal moments have been discussed for decades, only recently there is a marked interest in their characteristics,[18,20−22] and the design of proper structures that can sustain them under electromagnetic excitation.[23−25] Partly this is due to the weak far-field optical signatures of toroidal resonances. Usually, they do not radiate or their contribution is

Received: June 29, 2012
Revised: August 27, 2012
Published: August 30, 2012

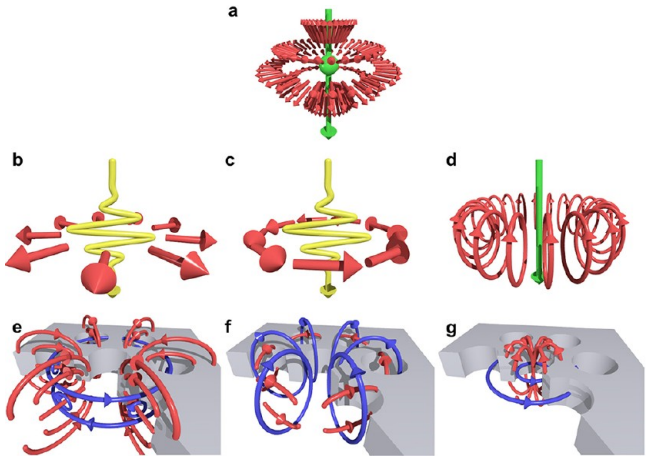

Figure 1. For excitation, we use (a) the relativistic field attached to the relativistic electrons in TEM and (b–d) optical excitations in FDTD: (b) radially and (c) azimuthally polarized far-field radiation, and (d) radiation emitted by an electric dipole placed in the central hole. The main classes of response fields sustained by the 6-fold torus are (e) radial electric dipolar and (f) radial magnetic dipolar, as well as (g) toroidal modes. Electric (magnetic) fields are indicated by red (blue) arrows.

masked by conventional multipolar far-field radiation.[26] In this context it is noteworthy that Kaelberer et al.[27] succeeded in observing toroidal moments using microwave split ring resonators, and Huang et al.[28] proposed an alternative structure which makes the toroidal resonances prominent at optical frequencies.

In this Letter, we present experimental and theoretical evidence for toroidal modes at visible frequencies, using energy-filtering transmission electron microscopy (EFTEM) and three-dimensional finite-difference time-domain analysis (3D-FDTD) of near- and far-field excitations. Our investigated structure consists of seven round holes of 60 nm diameter, drilled in a free-standing 60 nm thick silver film. First, silver discs with 3 mm diameter were punched from cold-rolled and annealed silver film. Afterwards the discs were electropolished in a Struers-Tenupol 5 by using a cyanide-free solution[29] until a hole was visible in the center of the disk. Voltage, current, and the light sensitivity value were set to 4 V, 25 mA, and 100, respectively. Finally the specimen was ion-milled at the Low-Angle Ion Milling & Polishing system (FISCHIONE Instruments-Model 1010) for final cleaning for an hour in total (at 2 kV for 30 min, at 0.5 kV for 30 min). A double beam was used at a milling angle of 12°. Both upper and lower sources were set to a current of 5 mA. The final thickness of the specimen was 60 ± 10 nm. The thickness measurement was done by comparing the areas below the zero loss peak and the total area in an electron energy-loss spectrum, namely the log–ratio method.[30]

The heptamer nanoholes consisting of seven circular holes (diameter = 60 nm) were drilled into the film by a focused ion beam (FIB) (FEI Nova NANOLAB 60) at 30 kV near the rim of the perforated area. The sub-electronvolt sub-angstrom microscope (SESAM, Zeiss, Oberkochen, Germany), operated at 200 kV, was used to implement the EFTEM experiments on the heptamer nanoholes. EFTEM is a technique based on electron energy-loss spectroscopy (EELS) and allows obtaining images formed by electrons having suffered specific energy losses in the material. The MANDOLINE energy filter and a symmetric electrostatic omega-type electron monochromator provide an energy resolution better than 100 meV, a high dispersion of the energy-loss spectrum (~6 μm/eV), and a small nonisochromaticity of 0.1 meV/nm.[31,32] During the EFTEM imaging procedure both the monochromator slit and energy filter slit had a width of 0.2 eV. Energy-filtered images were acquired at an energy loss step of 0.2 eV between 0 and 7 eV, and recorded on a $2k \times 2k$ CCD camera (Ultrascan, Gatan, USA) with a binning of 4. In order to exclude the camera artifacts due to scintillator afterglow, image acquisition was started from 7 eV, where the intensity is lowest, and was stopped at a value just below the intense zero-loss peak. In addition, a new dark reference was acquired after each energy-filtered image. The acquisition time was set automatically for each image with the constraint of a maximum time of 30 s to minimize image blurring stemming from specimen drift. The specimen drift between individual images was corrected by application of a script described in ref 33. The weighted principal component analysis (PCA) has been applied on the structure by selecting 14 components in order to reduce noise. To identify the exact energy positions of the weak spectral peaks in the data cube a peak-finding algorithm was written with Digital Micrograph scripting language. This is an essential tool for mapping the positions in the low-energy-loss region since there is no background function available for this energy region.[34] A bright-field image of the investigated structure is displayed in the Supporting Information Figure 1.

The 3D-FDTD method was used to simulate the electromagnetic behavior of heptamer holes. Yee's mesh was imposed on the structure and the edge length of the cubic cells used in order to discretize the structure was 2 nm. The dispersion of silver was based on a Drude model with two critical point functions. A Ricker wavelet was introduced as the temporal dependence of the incident beam for visualizing the plasmonic eigenmodes at different energies, as a Huygens source introduced in a plane 500 nm above the structure. For the spatial distribution of the excitation, different functions were used to efficiently decompose the symmetry of various modes. Near-field simulations were performed by placing an electric or magnetic dipole at the central hole in the structure to see the electrical and magnetic field distribution.

Our investigated structure consists of seven circular holes; a central hole is surrounded by a six-membered ring of holes. As this structure shares the D_{6h} symmetry[35] class with the benzene molecule and similar artificial plasmonic particle oligomers,[36–38] the group theoretical mode spectrum is the same in all cases. However, the topology of an oligomer of holes (a 6-fold toroid) is distinctly different from that of the complementary oligomer of separate particles. This promises an opportunity to discover eigenmodes in the toroidal system whose spatial structure does not resemble any mode of the discrete particle system.

EELS[10,39–42] and EFTEM[43–46] are quite advantageous in the study of plasmonic eigenmodes thanks to the unique spatial structure of the electromagnetic field attached to its relativistic electron probe, as illustrated in Figure 1a, acting as a near-field excitation source. It shares certain features, but is never identical, with various optical excitation field geometries (radial and azimuthal far-field, and dipolar near-field; Figure 1b–d). Using the varying degrees of overlap between electronic and optical excitations, their combined study yields a comprehensive understanding of a sample's eigenmodes. The principal resonances that can be observed with these excitation types are

dx.doi.org/10.1021/nl302418n | Nano Lett. 2012, 12, 5239–5244

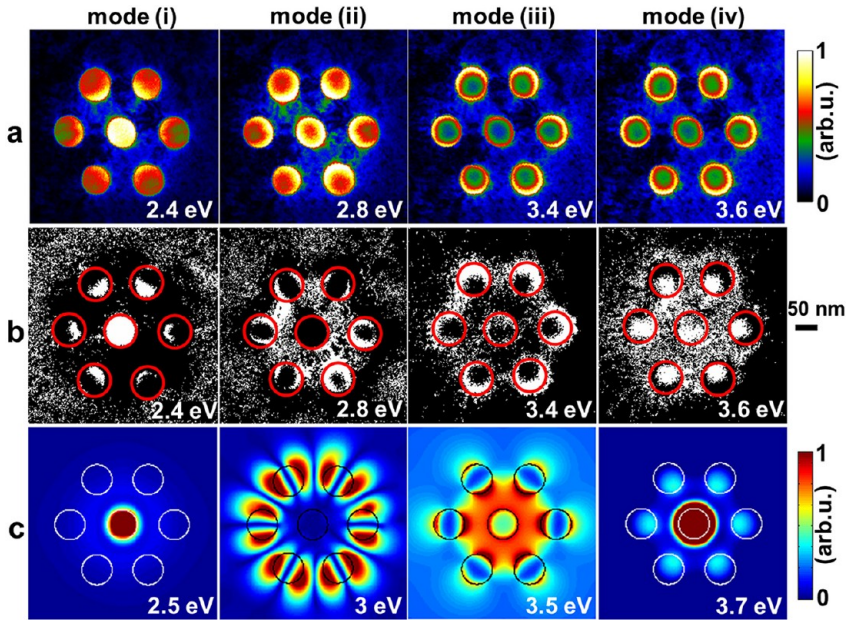

Figure 2. (a) Collection of modes acquired in EFTEM experiment at energy losses of (i) 2.4, (ii) 2.8, (iii) 3.4, and (iv) 3.6 eV. (b) Peak maps obtained from the acquired images in (a). (c) Simulated modes with FDTD. Displayed is the modulus of the electric field ($|E_z|$) at (i) 2.5, (ii) 3, (iii) 3.5, and (iv) 3.7 eV. The scale bar applies to all images.

illustrated in Figure 1e–g. Of particular interest in the present context are the toroidal modes, Figure 1g. Their weakly radiative character makes a near-field optical source compulsory, such as a vertical electric dipole emitter centered in the middle hole (Figure 1d). The simultaneous absence of near-field excitable resonances in far-field excited simulations is a fingerprint signature of toroidal modes, whose traces can be recognized in EFTEM experiments.

In Figure 2, we display EFTEM images (Figure 2a), corresponding peak maps (Figure 2b), and images from FDTD analysis (Figure 2c). Colors in Figure 2a represent the energy-loss probability, which is a measure of the *z*-component of the excited electric field, E_z. At an energy loss of 2.4 eV (mode (i)), intensity maxima are mainly concentrated in the central hole and along the inner rims of the surrounding holes indicating electromagnetic interaction in radial direction. At 2.8 eV (mode (ii)), electromagnetic interaction is observed between the surrounding holes in azimuthal direction. At 3.4 eV (mode (iii)) and 3.6 eV (mode (iv)), high field strengths are mainly observed along the outer rims of the surrounding holes. To unravel the symmetries of these resonances, peak maps (Figure 2b) are extracted from the EFTEM data cube (Figure 2a). Whereas EFTEM images show the E_z component at single energy slices, peak maps highlight the spatial distribution of spectral peaks, thus reducing the monotonous spectral tails of resonances at other energies. The peak maps of mode (i) and mode (iii) affirm the raw EFTEM images, indicating strong eigenmodes that are spectrally well isolated. In contrast, the peak maps at modes (ii) and (iv) differ noticeably from the corresponding EFTEM images. Associated resonances are relatively weaker and/or spectrally closer to other eigenmodes. The peak map of mode (ii) reveals clearly that the electromagnetic interaction between the surrounding holes is more pronounced in the azimuthal direction than in radial direction. The peak map of mode (iv) uncovers a shape that is not discernible in the corresponding EFTEM image, comprising peaks concentrated in the central hole and at the inner part of the surrounding holes. The resonance widths of modes (i) and (iv) are (0.4 ± 0.05) and (0.3 ± 0.05) eV, respectively.

Figure 2c highlights simulated images of the $|E_z|$ field component, obtained with different optical excitations as specified below. The spatial field distribution and the resonance energies are in very good agreement with experimental results (Figure 2a,b), lending assurance that FDTD calculations may be used to interpret mode structure. Most importantly, we will show in the following that the simulated modes (i) and (iv), observed at energy losses of 2.5 and 3.7 eV, respectively, are indeed toroidal resonances. In contrast, modes (ii) (at 3.0 eV) and (iii) (at 3.5 eV) are of prevailingly magnetic and electric dipolar nature, respectively.

Far-field simulations with radially polarized excitation reveal two prominent multipolar resonances at energies of 2.7 and 3.5 eV, respectively, shown in Figure 3. On the surface of the sample structure, electric field components oscillate in predominantly radial direction, accumulating opposite electrical charges on the inner and outer rim of the surrounding holes, which thus tend to behave like capacitors. Correspondingly, magnetic field vectors whirl in mostly azimuthal direction. Mode symmetry and energy identify the 3.5 eV resonance as mode (iii) from the EFTEM results (Figure 2a), whereas the calculated 2.7 eV mode appears to be masked in EFTEM by the eigenmode measured at 2.8 eV (Figure 2a). The reason for this suppression becomes clear, when the cross sectional symmetry is considered. As can be observed in Figure 3b, in the case of the 2.7 eV resonance the electric fields flip sign between the upper and lower substrate surfaces, giving rise to a quadrupolar plasmon mode.[47] At 3.5 eV, the electric fields do not differ in direction on the upper and lower surfaces (Figure 3e), giving this resonance a more easily excitable dipolar character.

An electromagnetically dual azimuthally polarized far-field excitation is introduced as well. The dominant response is found at 3 eV, as displayed in Figure 4, and can be associated with the EFTEM mode (ii) of Figure 2a. As expected, magnetic field components are aligned in radial direction. The electric

dx.doi.org/10.1021/nl302418n | *Nano Lett.* 2012, 12, 5239–5244

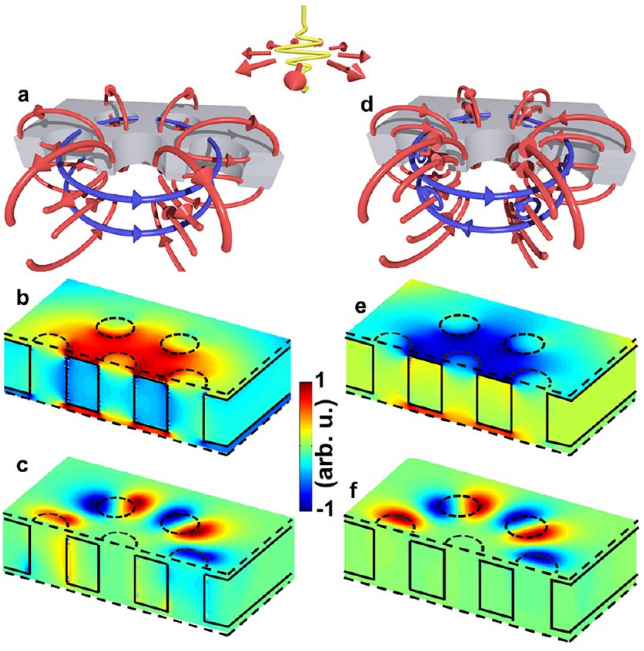

Figure 3. (a) Illustration of electric (red) and magnetic (blue) field lines, (b) instantaneous electric (E_z) and (c) instantaneous magnetic field strength (H_z) of the quadrupolar mode at 2.7 eV. (d) Illustration of field lines, (e) electric and (f) magnetic field strength of the dipolar mode at 3.5 eV. The color bar in the middle applies to (b,c,e,f). Field evaluations above and below the sample are done 4 nm away from the surface.

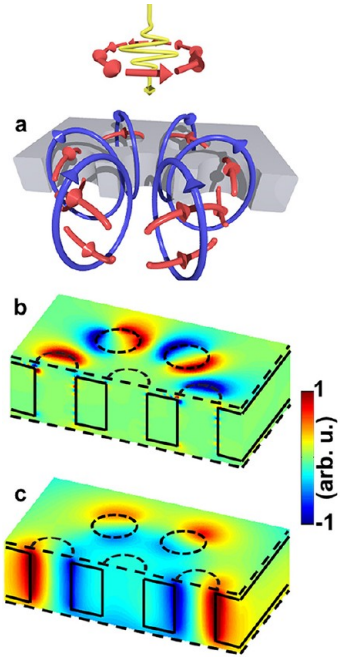

Figure 4. (a) Illustration of electric (red) and magnetic (blue) field lines, (b) instantaneous electric (E_z) and (c) instantaneous magnetic field strength (H_z) of the magnetic dipolar mode at 3 eV. The color bar applies to (b,c). Field evaluations above and below the sample are done 4 nm away from the surface.

fields point in preferentially azimuthal direction, but without z-components, which provide strong coupling to the traversing electron in EFTEM.

The simulations above were carried out with far-field excitations and did not trigger any observable toroidal resonances in the heptamer. In the main, the structure's far-field excitable resonances are rather mundane. They may be likened to a ring resonator exhibiting longitudinal and transverse modes in a chain of holes, much like the well-known Babinet complementary chain of particles.[48] However, modes (i) and (iv), which are clearly observed in EFTEM, are conspicuously missing in all the far-field simulations discussed so far. To explore these modes further, we introduce a near-field source for the FDTD simulations. An efficient excitation is provided by coupling a vertical dipole emitter in the middle of the central hole to the structure, as demonstrated in Figure 5.

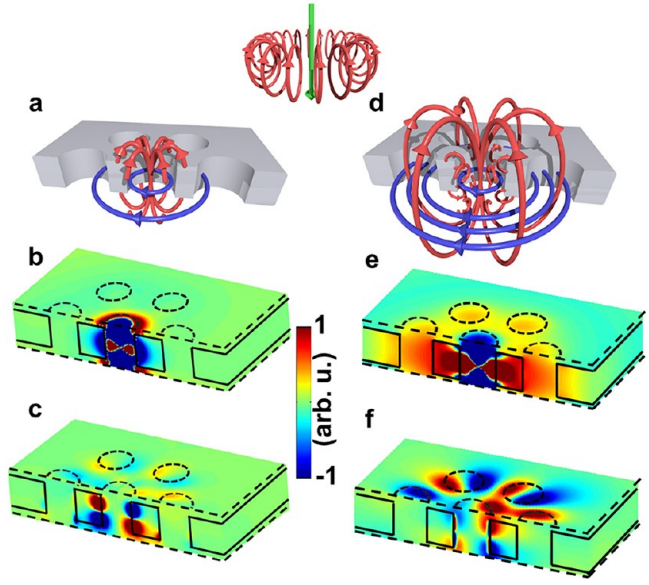

Figure 5. An electric dipole excitation was placed in the central hole. (a) Illustration of electric (red) and magnetic (blue) field lines, (b) instantaneous electric (E_z), and (c) instantaneous magnetic field strength (H_z) of the fundamental toroidal mode at 2.5 eV. (d) Illustration of field lines, (e) electric and (f) magnetic field strength of the second order toroidal mode at 3.7 eV. The color bar in the middle applies to (b,c,e,f). Field evaluations above and below the sample are done 4 nm away from the surface.

Our simulations with near-field excitation indeed verify resonances in the heptamer of holes at 2.5 and 3.7 eV, which is in excellent agreement with the experimentally found modes (i) and (iv) of Figure 2. Simulated near-field profile approves these resonances at 2.5 and 3.7 eV, also (Supporting Information Figure 2). The detailed analysis of field lines reveals a clearly toroidal character for both modes, illustrated in Figure 5a,d. The sample volume between the central and surrounding holes acts as a ring, around which toroidal moments can build up. The spokes that connect the ring to the outer bulk of the substrate evidently do not disrupt the topologically protected toroidal behavior. Magnetic field distributions (Figure 5c,f) encircle the central hole and electric fields flow in radial loops between the central and surrounding holes. The resonance at 3.7 eV is a higher-order toroidal mode. To illuminate further the toroidal character of these modes, we display in Figure 6 the optical currents extracted from our FDTD results. In both cases (Figure 6d,e), a cylindrical sheet of dipole moments is found to oscillate parallel to the symmetry axis of the sample. The currents are mostly concentrated in the supported silver ring

dx.doi.org/10.1021/nl302418n | *Nano Lett.* 2012, 12, 5239−5244

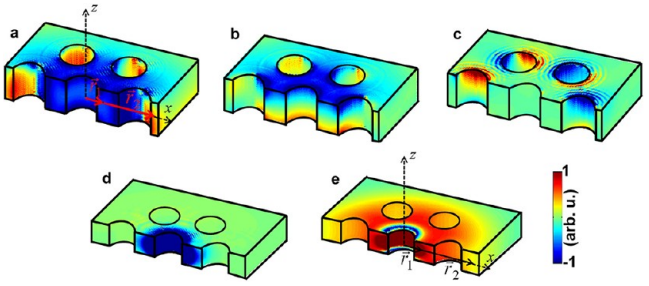

Figure 6. Moduli of the electric currents ($\vec{J}_z$) that build up the different modes at the energies of (a) E = 2.7 eV, (b) E = 3.5 eV, (c) E = 3 eV, (d) E = 2.5 eV, and (e) E = 3.7 eV, corresponding to quadrupolar radial, dipolar radial, azimuthal radial, and first and second toroidal modes, respectively.

surrounding the central hole, which results in strong toroidal moments, according to eq 1. It is evident why the azimuthal and radial electric dipole modes cannot result in a toroidal moment. The oscillation of the dephased currents violates the existence of a toroidal moment in z-direction. The resonance at E = 2.7 eV supports only a negligible toroidal moment, since $\vec{r}_1 \times (\vec{r}_1 \times \vec{J}(\vec{r}_1)) + \vec{r}_2 \times (\vec{r}_2 \times \vec{J}(\vec{r}_2)) \approx 0$ (see Figure 6). In contrast to the quadrupolar resonance, the toroidal resonances at E = 2.5 eV and E = 3.7 eV sustain a longitudinal current, localized at the silver ring separating the central hole from the other holes. For this reason, we believe that the distance between the central and the surrounding holes as well as the thickness of the silver film play an important role on the quality factor and resonance energy of the indicated toroidal mode.

The simulations above thus explain nicely all features observed in EFTEM. In addition, we have also considered the case of a dual[26] magnetic toroidal moment, which may be excitable by a magnetic dipole in the central hole instead of an electric dipole. The structure is expected to act in a complementary way, as if E and H are converted to H and $-E$, respectively.[49] Simulations revealed a possible resonance of such symmetry at 3.8 eV. However, at 3.8 eV the volume plasmon energy of silver dominates the spectral response making this toroidal mode experimentally inaccessible.

In summary, we have demonstrated the occurrence of toroidal moments at optical wavelengths for the first time experimentally. We have applied EFTEM imaging to a heptamer of circular holes in a silver film, arranged in such a way that between a central one and six surrounding holes a supported silver ring is formed. Thanks to the power of EFTEM, a number of eigenmodes of this ring structure could be visualized with nanometer spatial and a few tens of millielectronvolts spectral resolution. In particular, we observed radiation-free near-field optical features of two optically completely dark modes. FDTD simulations with a suitable near-field source revealed them to be toroidal resonances. Besides the fundamental toroidal mode at 2.4 eV also a higher order mode was found at 3.6 eV. Additional bright eigenmodes at 2.8 and 3.6 eV have multipolar characters.

Our present results demonstrate distinct toroidal resonances in the visible to ultraviolet spectral ranges. They are easily scalable to longer wavelengths, and we expect them to find many novel applications through innovative near-field optical engineering. For example, novel approaches to Fano spectral engineering by coupling toroidal dark and bright modes. This can be achieved, for example, by breaking the symmetry of the induced longitudinal currents by adding a substrate, or by breaking the azimuthal symmetry by altering the geometry of one of the outer holes.[50] A linear sequence of toroidal systems may constitute novel approaches to waveguides and resonators. Particle heptamers can be used to produce multiheptamer waveguide structures, along which magnetic plasmons propagate.[51] Also, coupling of single quantum systems to the near-fields of toroidal cavities should provide options for pronounced lifetime engineering via the Purcell-effect,[52−54] with implications for instance in quantum information storage and processing.[55−57]

■ ASSOCIATED CONTENT

Ⓢ Supporting Information

Additional figures. This material is available free of charge via the Internet at http://pubs.acs.org.

■ AUTHOR INFORMATION

Corresponding Author

*E-mail: ogut@is.mpg.de. Telephone: (711) 689-3637.

Notes

The authors declare no competing financial interest.

■ ACKNOWLEDGMENTS

We thank U. Eigenthaler and I. Lakemeyer for the support during the specimen preparation, C.T. Koch for writing the scripts regarding EFTEM acquisition and peak finding algorithm, and V. Fedotov for the fruitful discussions. N. Talebi gratefully acknowledges the Alexander-von-Humboldt foundation for financial support.

■ REFERENCES

(1) Anker, J. N.; Hall, W. P.; Lyandres, O.; Shah, N. C.; Zhao, J.; Van Duyne, R. P. *Nat. Mater.* **2008**, *7* (6), 442−453.
(2) Bardhan, R.; Lal, S.; Joshi, A.; Halas, N. J. *Acc. Chem. Res.* **2011**, *44* (10), 936−946.
(3) Tittl, A.; Mai, P.; Taubert, R.; Dregely, D.; Liu, N.; Giessen, H. *Nano Lett.* **2011**, *11* (10), 4366−4369.
(4) Lim, D.-K.; Jeon, K.-S.; Hwang, J.-H.; Kim, H.; Kwon, S.; Suh, Y. D.; Nam, J.-M. *Nat. Nanotechnol.* **2011**, *6* (7), 452−460.
(5) Linic, S.; Christopher, P.; Ingram, D. B. *Nat. Mater.* **2011**, *10* (12), 911−921.
(6) MacDonald, K. F.; Samson, Z. L.; Stockman, M. I.; Zheludev, N. I. *Nat. Photonics* **2009**, *3* (1), 55−58.
(7) Pendry, J. B.; Schurig, D.; Smith, D. R. *Science* **2006**, *312* (5781), 1780−1782.
(8) Vogelgesang, R.; Dmitriev, A. *Analyst* **2010**, *135* (6), 1175−1181.
(9) García de Abajo, F. J. *Rev. Mod. Phys.* **2007**, *79* (4), 1267−1290.
(10) Nelayah, J.; Kociak, M.; Stephan, O.; Garcia de Abajo, F. J.; Tence, M.; Henrard, L.; Taverna, D.; Pastoriza-Santos, I.; Liz-Marzan, L. M.; Colliex, C. *Nat. Phys.* **2007**, *3* (5), 348−353.
(11) Scholl, J. A.; Koh, A. L.; Dionne, J. A. *Nature* **2012**, *483* (7390), 421−427.
(12) Sonnefraud, Y.; Leen Koh, A.; McComb, D. W.; Maier, S. A. *Laser Photonics Rev.* **2011**, *6* (3), 277−295.
(13) Dorfmüller, J.; Vogelgesang, R.; Khunsin, W.; Rockstuhl, C.; Etrich, C.; Kern, K. *Nano Lett.* **2010**, *10* (9), 3596−3603.
(14) Liu, N.; Liu, H.; Zhu, S.; Giessen, H. *Nat. Photonics* **2009**, *3* (3), 157−162.
(15) Zel'dovich, I. B. *Sov. Phys. JETP* **1958**, *6*, 1184.
(16) Wood, C. S.; Bennett, S. C.; Cho, D.; Masterson, B. P.; Roberts, J. L.; Tanner, C. E.; Wieman, C. E. *Science* **1997**, *275* (5307), 1759−1763.
(17) Van Aken, B. B.; Rivera, J.-P.; Schmid, H.; Fiebig, M. *Nature* **2007**, *449* (7163), 702−705.

(18) Dubovik, V. M.; Tugushev, V. V. *Phys. Rep.* **1990**, *187* (4), 145−202.
(19) Spaldin, N. A.; Fiebig, M.; Mostovoy, M. *J. Phys.: Condens. Matter* **2008**, *20* (43), 434203.
(20) Radescu, E. E.; Vlad, D. H. *Phys. Rev. E* **1998**, *57* (5), 6030−6037.
(21) Radescu, E. E.; Vaman, G. *Phys. Rev. E* **2002**, *65* (4), 046609.
(22) Ederer, C.; Spaldin, N. A. *Phys. Rev. B* **2007**, *76* (21), 214404.
(23) Boardman, A. D.; Marinov, K.; Zheludev, N.; Fedotov, V. A. *Phys. Rev. E.* **2005**, *72* (1−6), 036603.
(24) Marinov, K.; Boardman, A. D.; Fedotov, V. A.; Zheludev, N. *New J. Phys.* **2007**, *9* (9), 324.
(25) Mary, A.; Dereux, A.; Ferrell, T. L. *Phys. Rev. B* **2005**, *72* (15), 155426.
(26) Jackson, J. D. *Classical Electrodynamics*; Wiley: New York, 1999.
(27) Kaelberer, T.; Fedotov, V. A.; Papasimakis, N.; Tsai, D. P.; Zheludev, N. I. *Science* **2010**, *330* (6010), 1510−1512.
(28) Huang, Y.-W.; Chen, W. T.; Wu, P. C.; Fedotov, V.; Savinov, V.; Ho, Y. Z.; Chau, Y.-F.; Zheludev, N. I.; Tsai, D. P. *Opt. Express* **2012**, *20* (2), 1760−1768.
(29) Lyles, R. L., Jr.; Rothman, S. J.; Jäger, W. *Metallography* **1978**, *11* (3), 361−363.
(30) Egerton, R. F. *Electron Energy-Loss Spectroscopy in the Electron Microscope*; Springer: New York, 2011.
(31) Koch, C. T.; Sigle, W.; Höschen, R.; Rühle, M.; Essers, E.; Benner, G.; Matijevic, M. *Microsc. Microanal.* **2006**, *12* (06), 506−514.
(32) Essers, E.; Benner, G.; Mandler, T.; Meyer, S.; Mittmann, D.; Schnell, M.; Höschen, R. *Ultramicroscopy* **2010**, *110* (8), 971−980.
(33) Schaffer, B.; Grogger, W.; Kothleitner, G. *Ultramicroscopy* **2004**, *102* (1), 27−36.
(34) Talebi, N.; Sigle, W.; Vogelgesang, R.; Koch, C. T.; Fernandez-Lopez, C.; Liz-Marzan, L. M.; Ögüt, B.; Rohm, M.; van Aken, P. A. *Langmuir* **2012**, *28* (24), 8867−8873.
(35) Hiberty, P. C.; Danovich, D.; Shurki, A.; Shaik, S. *J. Am. Chem. Soc.* **1995**, *117* (29), 7760−7768.
(36) Fan, J. A.; Wu, C.; Bao, K.; Bao, J.; Bardhan, R.; Halas, N. J.; Manoharan, V. N.; Nordlander, P.; Shvets, G.; Capasso, F. *Science* **2010**, *328* (5982), 1135−1138.
(37) Hentschel, M.; Saliba, M.; Vogelgesang, R.; Giessen, H.; Alivisatos, A. P.; Liu, N. *Nano Lett.* **2010**, *10* (7), 2721−2726.
(38) Liu, N.; Mukherjee, S.; Bao, K.; Brown, L. V.; Dorfmüller, J.; Nordlander, P.; Halas, N. J. *Nano Lett.* **2012**, *12* (1), 364−369.
(39) Batson, P. E. *Phys. Rev. Lett.* **1982**, *49* (13), 936−940.
(40) Rossouw, D.; Couillard, M.; Vickery, J.; Kumacheva, E.; Botton, G. A. *Nano Lett.* **2011**, *11* (4), 1499−1504.
(41) Liang, H.; Zhao, H.; Rossouw, D.; Wang, W.; Xu, H.; Botton, G. A.; Ma, D. *Chem. Mater.* **2012**, *24* (12), 2339−2346.
(42) von Cube, F.; Irsen, S.; Niegemann, J.; Matyssek, C.; Hergert, W.; Busch, K.; Linden, S. *Opt. Mater. Express* **2011**, *1* (5), 1009−1018.
(43) Nelayah, J.; Gu, L.; Sigle, W.; Koch, C. T.; Pastoriza-Santos, I.; Liz-Marzan, L. M.; van Aken, P. A. *Opt. Lett.* **2009**, *34*, 1003−1005.
(44) Schaffer, B.; Hohenester, U.; Trügler, A.; Hofer, F. *Phys. Rev. B* **2009**, *79*, 041401−1−4.
(45) Gu, L.; Sigle, W.; Koch, C. T.; Ögüt, B.; van Aken, P. A.; Talebi, N.; Vogelgesang, R.; Mu, J.; Wen, X.; Mao, J. *Phys. Rev. B* **2011**, *83*, 195433−1−7.
(46) Nicoletti, O.; Wubs, M.; Mortensen, N. A.; Sigle, W.; van Aken, P. A.; Midgley, P. A. *Opt. Express* **2011**, *19* (16), 15371−15379.
(47) Habteyes, T. G.; Dhuey, S.; Cabrini, S.; Schuck, P. J.; Leone, S. R. *Nano Lett.* **2011**, *11* (4), 1819−1825.
(48) Talebi, N.; Mahjoubfar, A.; Shahabadi, M. *J. Opt. Soc. Am. B* **2008**, *25* (12), 2116−2122.
(49) Harrington, R. F. *Time-harmonic electromagnetic fields*; McGraw-Hill: New York, 1961.
(50) Hentschel, M.; Dregely, D.; Vogelgesang, R.; Giessen, H.; Liu, N. *ACS Nano* **2011**, *5* (3), 2042−2050.
(51) Liu, N.; Mukherjee, S.; Bao, K.; Li, Y.; Brown, L. V.; Nordlander, P.; Halas, N. J. *ACS Nano* **2012**, *6* (6), 5482−5488.
(52) Altug, H.; Englund, D.; Vuckovic, J. *Nat. Phys.* **2006**, *2* (7), 484−488.
(53) Vahala, K. J. *Nature* **2003**, *424* (6950), 839−846.
(54) Koenderink, A. F. *Opt. Lett.* **2010**, *35* (24), 4208−4210.
(55) Choi, K. S.; Deng, H.; Laurat, J.; Kimble, H. J. *Nature* **2008**, *452* (7183), 67−71.
(56) Strauf, S.; Stoltz, N. G.; Rakher, M. T.; Coldren, L. A.; Petroff, P. M.; Bouwmeester, D. *Nat. Photonics* **2007**, *1* (12), 704−708.
(57) Hadfield, R. H. *Nat. Photonics* **2009**, *3* (12), 696−705.